Article

Désorite, Pb$_2$(Fe$^{3+}_6$Zn)O$_2$(PO$_4$)$_4$(OH)$_8$, a New Phosphate Mineral Isotypic with Jamesite

Anthony R. Kampf [1,*] , **Gerhard Möhn** [2] **and Chi Ma** [3]

1   Mineral Sciences Department, Natural History Museum of Los Angeles County, 900 Exposition Boulevard, Los Angeles, CA 90007, USA

2   Independent Researcher, Dr.-J.-Wittemannstrasse 5, 65527 Niedernhausen, Germany; gerhardmoehn705@gmail.com

3   Division of Geological and Planetary Sciences, California Institute of Technology, 1200 East California Boulevard, Pasadena, CA 91125, USA; chima@caltech.edu

*   Correspondence: akampf@nhm.org

Abstract: The new mineral désorite, Pb$_2$(Fe$^{3+}_6$Zn)O$_2$(PO$_4$)$_4$(OH)$_8$, is a secondary oxidation-zone mineral discovered on the dumps of the Schöne Aussicht mine, Dernbach, Westerwaldkreis, Rhineland-Palatinate, Germany. The crystals are irregular blades up to about 0.25 mm long, occurring in subparallel and radial aggregates. Désorite is brownish red. It has an orange streak, adamantine luster, brittle tenacity, splintery and curved fracture and two cleavages: {02$\overline{1}$} perfect and {001} good. It has a hardness (Mohs) of about 3 and is nonfluorescent in both long- and short-wave ultraviolet illumination. The calculated density is 4.633 g/cm^3. Optically, crystals are biaxial (+) with α = 2.00(1), β = 2.02(calc) and γ = 2.10(calc) (white light). The 2V is 54(2)° and the optical orientation is $Y \sim \perp$ {02$\overline{1}$}, $X \wedge$ **a** $\approx$ 13°. The mineral is pleochroic: X yellow brown, Y red brown, Z red brown; $X < Y \approx Z$. The empirical formula from electron microprobe analysis is Pb$_{1.93}$(Zn$_{0.50}$Fe$^{3+}_{6.29}$□$_{0.21}$)$_{\Sigma7.00}$(P$_{3.90}$As$_{0.10}$)$_{\Sigma4.00}$O$_{26}$H$_{8.28}$. Désorite is triclinic, space group $P\overline{1}$; the unit-cell parameters are a = 5.4389(7), b = 9.3242(13), c = 10.0927(12) Å, α = 109.024(8), β = 90.521(6), γ = 97.588(7)°, V = 478.90(11) Å^3 and Z = 1. Désorite has a framework structure (R_1 = 0.0487 for 937 $I > 2\sigma I$ reflections) assembled from Fe^{3+}O$_6$ octahedra and PO$_4$ tetrahedra, with Pb occupying cavities in the framework. The Fe^{3+}O$_6$ octahedra in the framework occur in edge-sharing chains, edge-sharing trimers and individual octahedra, all sharing corners with each other and with PO$_4$ tetrahedra. Désorite is isostructural with jamesite and lulzacite.

Keywords: désorite; new mineral; crystal structure; phosphate; jamesite; heteropolyhedral framework; Schöne Aussicht mine; Dernbach; Germany

1. Introduction

More than a century after its most active mining period, there is little evidence of the existence of the Schöne Aussicht mine near Dernbach, Germany. All that remains are overgrown dumps in a wooded area just west of the town. This certainly does not appear to be a very good spot to search for interesting minerals. Nevertheless, mineral collectors have scoured the area, often digging deep pits in hopes of turning up fresher dump material from the deposit's oxidation zone. One recent find netted the holotype specimen of the new mineral hanaueite, AgHgSI [1]. Herein, we report a second new mineral discovered at the locality—désorite.

The name désorite honours Joy Désor (b. 1990), for his tireless analytical work on mineral unknowns, which has led to the discovery and description of the new minerals ammoniotinsleyite, bojarite, oberwolfachite, oldsite, theuerdankite and hanaueite. Joy did the initial work that suggested that the new mineral described herein could be new. At Joy's suggestion, the name désorite also honours his noteworthy ancestor Pierre Jean Édouard Désor (1811–1882), a Swiss geologist and professor at Neuchâtel Academy (now

the University of Neuchâtel). He was a colleague of Louis Agassiz, among others. His studies on paleontology and glacial phenomena in Europe and North America are of particular note. He was a collaborator on the geological survey of the Lake Superior mineral district in the USA. (https://en.wikipedia.org/wiki/Pierre_Jean_%C3%89douard_Desor) (accessed on 2 February 2024).

The new mineral and its name have been approved by the International Mineralogical Association (IMA) Commission on New Minerals, Nomenclature and Classification (CNMNC) with the number 2023–087 and the symbol Dso. The description is based on one holotype specimen deposited in the collections of the Natural History Museum of Los Angeles County, 900 Exposition Boulevard, Los Angeles, CA 90007, USA, under catalogue number 76300.

2. Occurrence, Geological Setting and Mineral Association

Désorite was discovered on the dumps of the Schöne Aussicht mine, Dernbach, Westerwaldkreis, Rhineland-Palatinate, Germany ($50°27'15''$ N $07°46'25''$ E). (Note that there is another Schöne Aussicht mine near Burbach, North Rhine-Westphalia, Germany) The mine is the northernmost mine on the Emser Gangzug [2], which stretches northeast from Braubach (Rhine river), crossing the Lahn valley near Bad Ems, to Dernbach. The deposits are hydrothermal quartz-siderite veins usually containing the principal ore minerals sphalerite and galena (Ag-bearing), with minor chalcopyrite, pyrite and gersdorffite. The area belongs to the Rhenish Massif. The main mining period at the Schöne Aussicht mine was from 1850 to 1900. Mining took place down to a depth of 140 m. Lead was mined as cerussite and pyromorphite, and Fe as mixtures of iron oxides. The mine only exploited the oxidation zone; the primary ore zone was never reached. In contrast to the more southerly mines, including the mineral-rich Friedrichssegen mine, there is very little Cu and almost no Zn found at the Schöne Aussicht mine.

Désorite occurs in a secondary, oxidation-zone mineral assemblage in vugs in a goethite-quartz gossan in association with carminite, coronadite and plumbogummite. The obviously strongly oxidized nature of the assemblage and the deep brown-red color of désorite clearly indicate that all Fe in the mineral is in the 3+ state.

3. General Appearance, Physical, Chemical and Optical Properties

Désorite occurs as irregular blades up to about 0.25 mm long in subparallel and radial aggregates (Figures 1 and 2). The blades are flattened on $\{02\bar{1}\}$ and elongated and striated parallel to [100]. The observed crystal forms are $\{02\bar{1}\}$, $\{011\}$, $\{01\bar{2}\}$, $\{102\}$ and $\{10\bar{2}\}$ (Figure 3). No twinning was observed. The color of the mineral is brownish red. It has orange streaks, adamantine luster, brittle tenacity, splintery and curved fracture and two cleavages: $\{02\bar{1}\}$ excellent and $\{001\}$ good. The Mohs hardness based on scratch tests is about 3. The mineral is nonfluorescent in both long- and short-wave ultraviolet illumination. The density could not be measured because crystals exceed the density of available density fluids. The calculated density based on the empirical formula and single-crystal cell is 4.633 g/cm^3. The mineral is insoluble in room-temperature concentrated HCl.

Optically, crystals are biaxial (+) with α = 2.00(1), β = 2.02(calc), γ = 2.10(calc), measured in white light. The 2V determined from extinction data using EXCALIBRW (version 5.0) [3] is 54(2)°. Note that γ was calculated from the γ–α birefringence (0.10) measured with a Berek compensator and β was then calculated from α, γ and 2V. The dispersion could not be observed. The optical orientation is $Y \sim \perp \{02\bar{1}\}$, $X \wedge$ **a** $\approx 13°$. The mineral is strongly pleochroic: X yellow brown, Y red brown, Z red brown; $X < Y \approx Z$.

The Gladstone–Dale compatibility [4] $1 - (K_p/K_c)$ = −0.001 (superior) based on the empirical formula.

Figure 1. Sprays of désorite blades (bright brownish red) on goethite (darker balls) on holotype specimen 76,300; the field of view is 3.35 mm across.
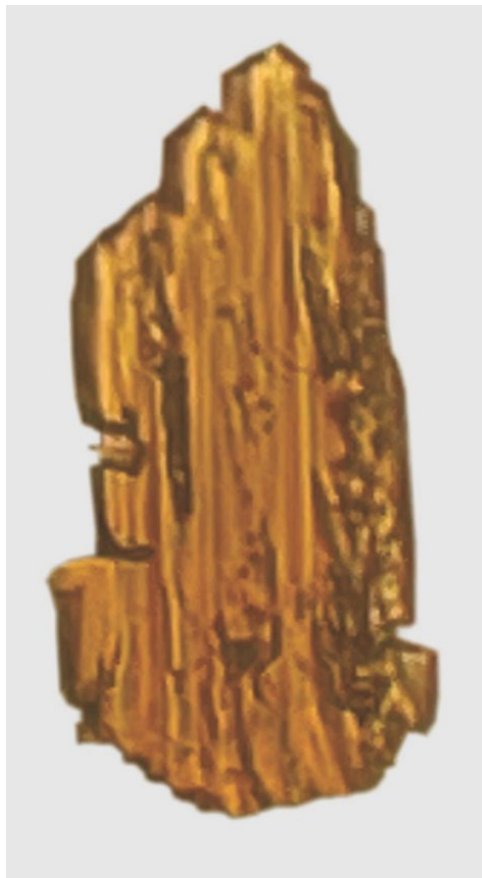

Figure 2. Désorite crystal (70 × 40 × 5 μm) used for the collection of structure data, viewed in plane polarized light (∣∣X).
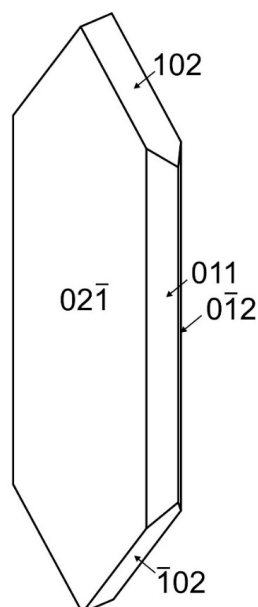
Figure 3. Crystal drawing of désorite; clinographic projection in nonstandard orientation, **a** vertical.

4. Chemical Composition

Analyses (12 points on 2 crystals) were performed at Caltech on a JEOL JXA-iHP200F field-emission electron microprobe (EPMA) in WDS mode. Analytical conditions were 15 kV accelerating voltage, 10 nA beam current and 5 μm beam diameter. Insufficient material was available for the determination of H_2O, so it was calculated based on the structure (O = 26 and P + As = 4). The crystals did not take a good polish, resulting in a relatively low analytical total. Analytical data are given in Table 1. Note that attempts to record Raman spectra using 532 and 785 nm lasers failed because of the sensitivity of désorite to the lasers even at low power.

Table 1. Chemical composition (wt%) for désorite.

Constituent	Mean	Range	S.D.	Standard/Line	Normalized
PbO	30.92	30.53–31.34	0.23	PbS/Pb $M\alpha$	32.24
ZnO	2.91	2.59–3.06	0.15	ZnO/Zn $K\alpha$	3.04
Fe_2O_3	36.02	35.49–36.76	0.46	Fayalite/Fe $K\alpha$	37.57
As_2O_5	0.84	0.62–0.87	0.08	GaAs/As $K\alpha$	0.88
P_2O_5	19.85	18.67–19.65	0.40	apatite/P $K\alpha$	20.70
H_2O *	5.35				5.58
Total	95.89				100.01

* Based on the structure (O = 26 and P + As = 4).

The empirical formula (based on 26 O *apfu*) is $Pb_{1.93}(Zn_{0.50}Fe^{3+}_{6.29}\square_{0.21})_{\Sigma7.00}(P_{3.90}As_{0.10})_{\Sigma4.00}O_{26}H_{8.28}$. The simplified formula is $Pb_2(Fe^{3+},Zn,\square)_7O_2[(P,As)O_4]_4(OH)_8$. The ideal formula is $Pb_2(Fe^{3+}_6Zn)O_2(PO_4)_4(OH)_8$ which requires PbO 32.76, ZnO 5.97, Fe_2O_3 35.15, P_2O_5 20.83, H_2O 5.29, total 100 wt%.

5. X-ray Diffraction

X-ray powder diffraction (PXRD) data were recorded using a Rigaku R-Axis Rapid II curved imaging plate microdiffractometer with monochromatized Mo$K\alpha$ radiation. The sample consisted of an aggregate of several crystals and a Gandolfi-like motion on the φ and ω axes was used to further randomize the sample. Observed *d* values and intensities were derived by profile fitting using JADE Pro (version 8.9) (Materials Data, Inc., Livermore,

CA, USA). Data are given in Table 2 and the match between the observed and calculated PXRDs is shown in Figure 4. The triclinic (space group $P\bar{1}$) unit-cell parameters refined from the powder data using JADE Pro with whole pattern fitting were a = 5.438(7), b = 9.327(7), c = 10.088(7) Å, α = 109.02(3), β = 90.561(2), γ = 97.62(3)° and V = 478.7(8) Å^3.

Table 2. Powder X-ray diffraction data (d in Å) for désorite. Only calculated lines with $I \geq 2.5$ are listed.

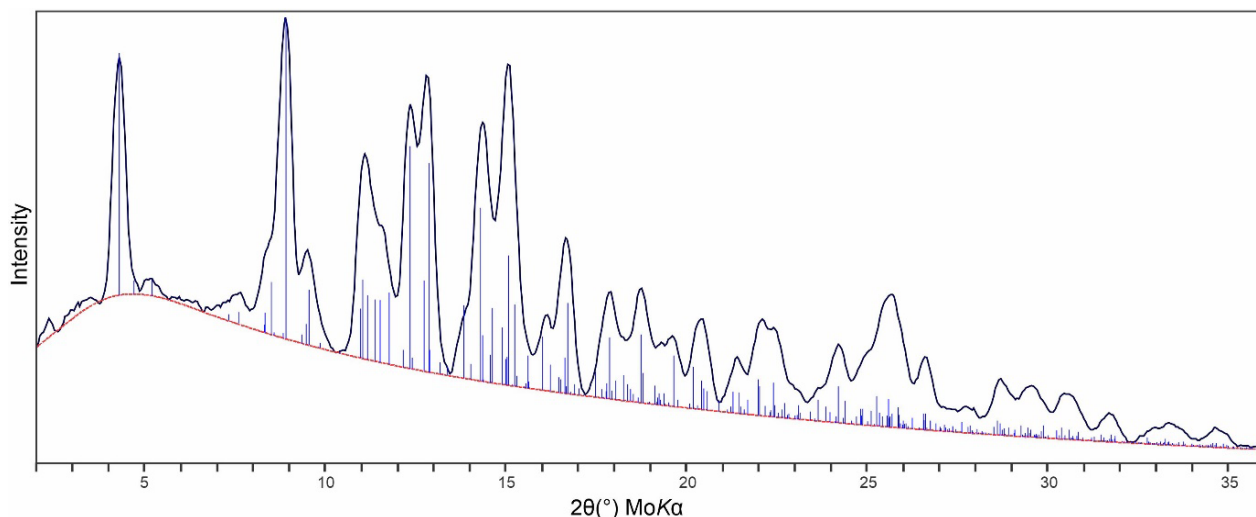| I_{obs}	d_{obs}	d_{calc}	I_{calc}	hkl	I_{obs}	d_{obs}	d_{calc}	I_{calc}	hkl	I_{obs}	d_{obs}	d_{calc}	I_{calc}	hkl
72	9.492	9.527	65	0 0 1			2.298	9	0 $\bar{4}$ 1			1.624	10	0 5 1
—	—	8.725	5	0 1 0	27	2.283	2.289	17	2 0 2	30	1.613	1.619	5	2 $\bar{5}$ 1
6	7.872	7.854	5	0 $\bar{1}$ 1			2.281	3	$\bar{1}$ $\bar{3}$ 3			1.615	3	3 $\bar{3}$ 2
9	5.328	5.383	3	1 0 0	—	—	2.266	6	1 $\bar{1}$ 4			1.604	16	$\bar{2}$ 2 4
24	4.862	4.905	7	$\bar{1}$ 1 0	15	2.231	2.240	8	0 2 3	31	1.593	1.601	3	$\bar{3}$ 0 3
		4.802	14	$\bar{1}$ 0 1			2.226	5	1 $\bar{4}$ 1			1.598	5	$\bar{2}$ 0 5
100	4.584	4.580	100	0 $\bar{2}$ 1	—	—	2.218	4	$\bar{1}$ 2 4			1.587	11	2 4 0
29	4.273	4.314	6	1 1 0	35	2.181	2.182	21	0 3 2	14	1.574	1.579	7	1 $\bar{3}$ 6
		4.278	16	$\bar{1}$ $\bar{1}$ 1			2.175	9	2 $\bar{3}$ 1			1.564	4	$\bar{3}$ 1 3
59	3.687	3.722	14	1 $\bar{2}$ 1	16	2.126	2.139	6	$\bar{2}$ $\bar{2}$ 2	24	1.543	1.546	9	$\bar{1}$ 0 6
		3.699	22	0 1 2			2.126	8	0 1 4			1.543	6	1 $\bar{5}$ 5
		3.655	20	1 1 1			2.112	4	1 $\bar{3}$ 4			1.536	3	1 $\bar{6}$ 2
29	3.573	3.590	18	$\bar{1}$ $\bar{1}$ 2	20	2.082	2.082	16	1 $\bar{4}$ 3	7	1.511	1.527	3	0 $\bar{6}$ 3
		3.548	17	0 2 1	17	2.021	2.027	13	$\bar{1}$ $\bar{3}$ 4			1.514	3	1 $\bar{6}$ 1
27	3.483	3.473	21	1 0 2	20	1.996	2.005	9	0 $\bar{1}$ 5	8	1.484	1.488	4	$\bar{1}$ 5 2
—	—	3.362	5	0 $\bar{1}$ 3			1.999	7	2 0 3	5	1.465	1.475	4	$\bar{1}$ 5 5
79	3.307	3.305	68	1 $\bar{2}$ 2			1.990	6	1 2 3			1.442	3	$\bar{2}$ 4 3
90	3.183	3.208	28	$\bar{1}$ 1 2	—	—	1.959	4	2-3 3	17	1.436	1.437	5	$\bar{3}$ 4 1
		3.175	67	1 2 0	17	1.916	1.923	7	1 1 4			1.433	5	0 $\bar{5}$ 6
—	—	3.100	3	0 $\bar{2}$ 3			1.908	9	0-3 5			1.428	3	$\bar{2}$ $\bar{2}$ 6
17	2.944	2.953	21	0 $\bar{3}$ 2	11	1.873	1.888	5	$\bar{2}$ $\bar{3}$ 2	9	1.419	1.422	3	$\bar{2}$ 5 3
—	—	2.911	4	1 1 2	24	1.854	1.863	21	1 $\bar{1}$ 5			1.414	3	2 1 5
79	2.850	2.856	66	$\bar{1}$ $\bar{1}$ 3			1.847	3	0 $\bar{5}$ 2			1.406	5	2 $\bar{6}$ 1
—	—	2.804	8	$\bar{1}$ 0 3	25	1.821	1.835	4	$\bar{2}$ 0 4	14	1.398	1.397	5	$\bar{1}$ $\bar{2}$ 7
32	2.775	2.792	22	1 2 1			1.828	15	$\bar{1}$ 0 5			1.393	3	$\bar{1}$ 4 4
97	2.707	2.743	17	1 $\bar{2}$ 3			1.809	3	$\bar{3}$ 1 0	11	1.382	1.377	5	2 5 0
		2.710	55	0 1 3	—	—	1.804	5	$\bar{2}$ $\bar{3}$ 3	5	1.360	1.361	3	0 0 7
		2.682	25	$\bar{2}$ 1 0	—	—	1.797	3	$\bar{1}$ $\bar{4}$ 4	14	1.349	1.355	4	0 2 6
—	—	2.671	3	1 0 3	10	1.780	1.774	8	0 4 2			1.346	5	4 0 0
12	2.631	2.618	12	0 $\bar{3}$ 3	—	—	1.750	3	$\bar{3}$ 2 0	7	1.333	1.335	4	2 0 6
23	2.537	2.551	16	$\bar{2}$ 1 1	9	1.736	1.734	7	$\bar{1}$ 5 0			1.309	3	0-6 6
		2.519	8	0 $\bar{1}$ 4	11	1.706	1.719	5	$\bar{3}$ $\bar{1}$ 1	11	1.301	1.298	5	1 $\bar{7}$ 1
—	—	2.484	5	$\bar{2}$ $\bar{1}$ 1			1.710	3	3 1 0			1.294	4	0 $\bar{7}$ 4
—	—	2.474	4	2 1 0	19	1.690	1.695	15	1 3 3	6	1.253	1.259	3	0 $\bar{2}$ 8
50	2.452	2.456	13	2 $\bar{2}$ 1			1.681	9	0 $\bar{2}$ 6	8	1.232	1.241	4	$\bar{1}$ $\bar{7}$ 2
		2.446	28	$\bar{1}$ 3 1	13	1.656	1.661	3	$\bar{1}$ $\bar{5}$ 1			1.223	3	$\bar{2}$ 6 2
—	—	2.418	3	1 3 0			1.653	8	2 $\bar{4}$ 4					
12	2.314	2.339	8	$\bar{2}$ $\bar{1}$ 2	16	1.637	1.649	6	3 $\bar{3}$ 1					
		2.315	3	2 1 1			1.633	5	$\bar{1}$ $\bar{4}$ 5					

Figure 4. Comparison of the observed (solid black line) and calculated (thin blue vertical lines) PXRDs for désorite.

The small size and less-than-ideal quality of the crystal limited the dataset, providing a low data-to-parameter ratio of 6.27. The Rigaku CrystalClear (version 2.0) software package was used for processing the structure data, including the application of an empirical absorption correction using the multi-scan method with ABSCOR [5] implemented within CrystalClear. The structure was solved using the intrinsic-phasing algorithm of SHELXT-2014/5 [6]. SHELXL-2016/6 [7] was used for the refinement of the structure. The structure solution in space group $P\bar{1}$ located all cation and O sites.

With all O sites assigned full occupancy, an initial refinement indicated the Pb site to be split into two sites about 0.6 Å apart. These eventually were refined to occupancies of 0.72(3) for PbA and 0.27(3) for PbB with a separation of 0.62(3) Å. The two P sites (P1 and P2) were refined with joint occupancy by P and As, eventually refining to P1: $P_{0.996(12)}As_{0.004(12)}$ and P2: $P_{0.970(11)}As_{0.030(11)}$. The occupancies of five Fe sites (Fe1, Fe2, Fe3, Fe4 and Fe5) were refined to 1.016(13), 0.983(13), 1.000(13), 0.994(10) and 0.977(9).

To assess the distribution of Fe^{3+}, Zn and vacancies among the Fe sites, we employed the program OccQP (version 0.39) [8], which uses quadratic equations in a constrained least-squares formulation to optimize occupancy assignments based upon site scattering, chemical composition, charge balance, bond valence and cation–anion bond lengths. In the OccQP analysis, the chemical composition (based on the empirical formula), bond valence and site scattering were all allowed to vary with equal weighting. The OccQP-calculated occupancies for the Fe sites (Table 3) were used in the final structure refinement. The final structural formula with the Fe sites combined is $Pb_{1.98}(Fe^{3+}_{6.30}Zn_{0.56}\square_{0.14})O_2[(P_{0.98}As_{0.02})O_4]_4(OH)_8$. Note that H atoms were included based on the bond-valence analysis even though H sites could not be located. Without the location of H sites, the hydrogen bonding was somewhat ambiguous. Each of the OH sites could conceivably form H bonds to more than one receptor O site. We have listed all of these and have assigned factored bond valences.

Table 3. Results of the OccQP analysis for désorite.

Site	Site Scattering Values *		Site Occupancies According to *OccQP*
	Refinement	***OccQP***	
Fe1	26.351	26.326	$Fe^{3+}_{0.919}Zn^{2+}_{0.081}$
Fe2	25.579	25.579	$Fe^{3+}_{0.984}\square_{0.016}$
Fe3	25.964	25.962	$Fe^{3+}_{0.600}Zn^{2+}_{0.350}\square_{0.050}$
Fe4	51.704	51.700	$Fe^{3+}_{0.920}Zn^{2+}_{0.065}\square_{0.015}$
Fe5	50.830	50.830	$Fe^{3+}_{0.978}\square_{0.022}$

* Site scattering value = mean atomic number $\times$ site multiplicity.

The data collection and refinement details are given in Table 4, atom coordinates and displacement parameters in Table 5, selected bond distances in Table 6 and a bond-valence analysis in Table 7.

Table 4. Data collection and structure refinement details for désorite.

Diffractometer	Rigaku R-Axis Rapid II	
X-ray radiation	Mo$K\alpha$ (λ = 0.71075 Å)	
Temperature	293(2) K	
Structural formula (incl. unlocated H)	$Pb_{1.98}(Fe^{3+}_{6.30}Zn_{0.56}\square_{0.14})O_2[(P_{0.98}As_{0.02})O_4]_4(OH)_8$	
Space group	*P*-1 (#2)	
Unit-cell dimensions	*a* = 5.4389(7) Å	α = 109.024(8)°
	b = 9.3242(13) Å	β = 90.521(6)°
	c = 10.0927(12) Å	γ = 97.588(7)°
V	478.90(11) Å^3	
Z	1	
Density (for above formula)	4.680 g·cm^{-3}	
Absorption coefficient	23.234 mm^{-1}	
F(000)	620.2	
Crystal size	70 $\times$ 40 $\times$ 5 mm	
θ range	3.65 to 22.37°	
Index ranges	$-5 \leq h \leq 5, -9 \leq k \leq 9, -10 \leq l \leq 10$	
Reflections collected/unique	2729 / 1213; R_{int} = 0.076	
Reflections with $I > 2\sigma I$	937	
Completeness to θ = 22.37°	99.10%	
Refinement method	Full-matrix least-squares on F^2	
Parameters/restraints	195 / 0	
GoF	1.026	
Final *R* indices [$I > 2\sigma I$]	R_1 = 0.0485, wR_2 = 0.0999	
R indices (all data)	R_1 = 0.0670, wR_2 = 0.1096	
Extinction coefficient	0.0007(6)	
Largest diff. peak/hole	+1.45 / −1.70 e/A^3	

R_{int} = S$|F_o^2 - F_o^2(mean)|$/S$[F_o^2]$. GoF = S = $\{S[w(F_o^2 - F_c^2)^2]/(n-p)\}^{1/2}$. R_1 = S$||F_o| - |F_c||$/S$|F_o|$. wR_2 = $\{S[w(F_o^2 - F_c^2)^2]/S[w(F_o^2)^2]\}^{1/2}$; w = 1/$[s^2(F_o^2)+(aP)^2+bP]$ where a is 0.0541, b is 1.6 and P is $[2F_c^2+Max(F_o^2,0)]/3$.

Table 5. Atom coordinates and displacement parameters (Å^2) for désorite.

	x/a	*y/b*	*z/c*	U_{eq}	**Occupancy**
PbA	0.4299(15)	0.7603(4)	0.5712(3)	0.0284(11)	$Pb_{0.72(3)}$
PbB	0.322(6)	0.7347(19)	0.5774(8)	0.048(4)	$Pb_{0.27(3)}$
Fe1	0	0	0.5	0.0241(10)	$Fe_{0.919}Zn_{0.081}$
Fe2	0	0.5	0	0.0150(9)	$Fe_{0.984}$
Fe3	0.5	0	0	0.0162(9)	$Fe_{0.600}Zn_{0.345}$

Table 5. *Cont.*

	x/a	*y/b*	*z/c*	U_{eq}	**Occupancy**	
Fe4	0.7445(4)	0.6325(3)	0.2812(2)	0.0166(7)	Fe$_{0.920}$Zn$_{0.065}$	
Fe5	0.0047(4)	0.0769(3)	0.1691(2)	0.0191(8)	Fe$_{0.978}$	
P1	0.1984(7)	0.4349(5)	0.2747(4)	0.0172(19)	P$_{0.996(12)}$As$_{0.004(12)}$	
P2	0.2909(7)	0.8195(5)	0.2310(4)	0.0130(17)	P$_{0.970(11)}$As$_{0.030(11)}$	
O1	0.9884(18)	0.5143(13)	0.3460(10)	0.022(3)	1	
O2	0.1885(16)	0.2756(14)	0.2902(10)	0.020(3)	1	
O3	0.1986(17)	0.4149(13)	0.1155(10)	0.018(3)	1	
O4	0.4520(19)	0.5258(13)	0.3502(10)	0.023(3)	1	
O5	0.5181(18)	0.7393(14)	0.1903(10)	0.021(3)	1	
O6	0.2762(18)	0.8865(14)	0.3921(10)	0.026(3)	1	
O7	0.3011(18)	0.9521(13)	0.1683(10)	0.022(3)	1	
O8	0.0440(17)	0.7060(13)	0.1678(10)	0.020(3)	1	
O9	0.7863(17)	0.8008(12)	0.4547(9)	0.016(3)	1	
OH10	0.2947(17)	0.5496(12)	0.9041(9)	0.018(3)	1	
OH11	0.1322(16)	0.9748(12)	0.6758(9)	0.015(3)	1	
OH12	0.7086(17)	0.1769(13)	0.1398(9)	0.019(3)	1	
OH13	0.8065(19)	0.8984(13)	0.0090(10)	0.021(3)	1	
	U^{11}	U^{22}	U^{33}	U^{23}	U^{13}	U^{12}
PbA	0.029(2)	0.0385(11)	0.0199(8)	0.0094(6)	0.0064(9)	0.0120(12)
PbB	0.057(10)	0.049(4)	0.034(2)	0.003(2)	0.014(3)	0.026(5)
Fe1	0.0222(19)	0.026(2)	0.0230(18)	0.0042(16)	0.0121(15)	0.0100(16)
Fe2	0.0141(17)	0.021(2)	0.0103(16)	0.0053(14)	0.0023(14)	0.0045(15)
Fe3	0.0097(16)	0.021(2)	0.0170(16)	0.0049(14)	0.0013(14)	0.0029(14)
Fe4	0.0123(13)	0.0241(17)	0.0128(12)	0.0045(11)	0.0034(10)	0.0048(11)
Fe5	0.0140(13)	0.0252(17)	0.0168(12)	0.0048(11)	0.0002(10)	0.0039(11)
P1	0.014(3)	0.028(3)	0.012(2)	0.009(2)	0.0015(18)	0.004(2)
P2	0.009(2)	0.022(3)	0.008(2)	0.0054(18)	0.0026(16)	0.0035(18)
O1	0.015(6)	0.040(8)	0.017(6)	0.013(5)	0.002(5)	0.014(6)
O2	0.004(5)	0.041(9)	0.014(5)	0.008(5)	−0.002(4)	−0.001(5)
O3	0.016(6)	0.025(7)	0.013(5)	0.003(5)	−0.003(5)	0.008(5)
O4	0.028(6)	0.033(8)	0.013(5)	0.012(5)	−0.002(5)	0.006(6)
O5	0.016(5)	0.036(8)	0.016(6)	0.015(5)	0.002(5)	0.003(5)
O6	0.021(6)	0.048(9)	0.011(5)	0.011(6)	0.007(5)	0.012(6)
O7	0.019(6)	0.017(7)	0.029(6)	0.007(5)	0.014(5)	−0.001(5)
O8	0.017(6)	0.021(7)	0.018(5)	0.002(5)	0.003(5)	0.008(5)
O9	0.018(5)	0.016(7)	0.010(5)	−0.003(5)	0.008(5)	0.003(5)
OH10	0.019(6)	0.023(8)	0.011(5)	0.002(5)	−0.002(5)	0.006(5)
OH11	0.010(5)	0.024(7)	0.015(5)	0.009(5)	0.006(5)	0.003(5)
OH12	0.010(5)	0.038(8)	0.006(5)	0.004(5)	0.002(4)	−0.001(5)
OH13	0.022(6)	0.031(8)	0.013(5)	0.010(5)	0.004(5)	0.008(5)

Table 6. Selected bond distances (Å) for désorite.

PbA–O9	2.328(13)	Fe1–O9 (×2)	1.969(10)	P1–O1	1.504(11)
PbA–O4	2.582(11)	Fe1–OH11 (×2)	2.004(9)	P1–O2	1.538(13)
PbA–O2	2.610(10)	Fe1–O6 (×2)	2.064(10)	P1–O3	1.556(10)
PbA–O6	2.640(11)	<Fe1–O>	2.012	P1–O4	1.566(11)
PbA–OH11	2.692(11)			<P1–O>	1.541
PbA–OH12	2.909(10)	Fe2–OH10 (×2)	1.961(10)		
PbA–O4	3.159(11)	Fe2–O3 (×2)	1.990(10)	P2–O5	1.519(11)
PbA–O7	3.247(11)	Fe2–O8 (×2)	2.089(10)	P2–O6	1.547(10)
PbA–O1	3.353(12)	<Fe2–O>	2.013	P2–O7	1.557(12)
PbA–O6	3.367(13)			P2–O8	1.581(10)
PbA–O1	3.511(13)	Fe3–OH12 (×2)	1.990(10)	<P2–O>	1.551

Table 6. *Cont.*

PbA–O2	3.671(13)	Fe3–OH9 (×2)	2.038(11)		
<PbA–O>	3.006	Fe3–O7 (×2)	2.158(10)	Hydrogen bonds	
		<Fe3–O>	2.062	OH10···O3	2.749(13)
PbB–OH11	2.499(14)			OH10···O5	2.998(13)
PbB–O4	2.651(15)	Fe4–O9	1.921(9)	OH10···OH12	2.728(16)
PbB–OH12	2.714(13)	Fe4–O4	2.016(11)	OH11···O5	2.970(14)
PbB–O6	2.715(16)	Fe4–O1	2.060(10)	OH11···O6	2.896(14)
PbB–O9	2.90(3)	Fe4–O5	2.061(10)	OH11···O9	2.807(15)
PbB–O1	2.96(2)	Fe4–OH10	2.062(10)	OH12···O7	2.943(13)
PbB–O2	2.99(3)	Fe4–O8	2.164(10)	OH12···OH10	2.728(16)
PbB–O1	3.00(3)	<Fe4–O>	2.047	OH13···O3	2.775(16)
PbB–O2	3.10(3)			OH13···O5	3.036(14)
PbB–O4	3.141(13)	Fe5–OH11	1.911(9)		
PbB–O9	3.36(3)	Fe5–O2	1.984(11)		
PbB–O7	3.57(3)	Fe5–OH12	2.030(11)		
<PbB–O>	2.967	Fe5–OH9	2.070(10)		
		Fe5–O7	2.108(11)		
		Fe5–OH9	2.140(10)		
		<Fe5–O>	2.041		

Table 7. Bond-valence analysis for désorite. Values are expressed in valence units *.

	PbA	PbB	Fe1	Fe2	Fe3	Fe4	Fe5	P1	P2	Hydrogen Bonds		Σ
										Donated	Accepted	
O1	0.04, 0.03	0.04, 0.03				0.43		1.31				1.88
O2	0.19, 0.02	0.03, 0.03					0.53	1.2				2.00
O3				0.53 ×2↓				1.14			0.07, 0.10	1.84
O4	0.20, 0.06	0.07, 0.02				0.49		1.11				1.95
O5						0.43			1.28		0.04, 0.05, 0.06	1.86
O6	0.18, 0.04	0.06	0.43 ×2↓						1.19		0.05	1.95
O7	0.05	0.01			0.30 ×2↓		0.38	1.15			0.07	1.96
O8				0.40 ×2↓		0.32		1.08				1.80
O9	0.34	0.04, 0.02	0.56 ×2↓			0.63					0.06	1.65
OH10				0.57 ×2↓		0.43				−0.07, −0.04, −0.07	0.11	0.93
OH11	0.16	0.09	0.51 ×2↓				0.65			−0.05, −0.05, −0.06		1.26
OH12	0.10	0.06			0.48 ×2↓		0.47			−0.07, −0.11	0.07	1.00
OH13					0.42 ×2↓		0.42, 0.35			−0.10, −0.06		1.04
Σ	1.41	0.50	3.00	3.00	2.40	2.73	2.80	4.76	4.7			

* Bond valence parameters are from [9]; hydrogen-bond strengths based on O–O bond lengths from [10]. Note that bond-valence values are based on the occupancies of the sites.

6. Description of Crystal Structure

Désorite has a framework structure assembled from edge- and corner-sharing $Fe^{3+}O_6$ octahedra and PO_4 tetrahedra. Fe3- and Fe5-centered octahedra share edges to form a chain

that alternates between one and two octahedra wide. Fe2- and Fe4-centered octahedra share edges to form a linear trimer. These tightly bonded units are linked to each other by sharing corners with a single Fe1-centered octahedron, thereby forming an octahedral framework. The PO$_4$ tetrahedra, centered by P1 and P2, form additional linkages between the octahedral units. The Pb, split between two sites separated by 0.62(3) Å, occupies cavities within the framework and bonds to surrounding O and OH sites. The octahedral units and their linkages to one another and with the phosphate tetrahedra are shown in a slice of structure viewed perpendicularly to {02$\bar{1}$} in Figure 5. The entire structure viewed along [100] is shown in Figure 6.
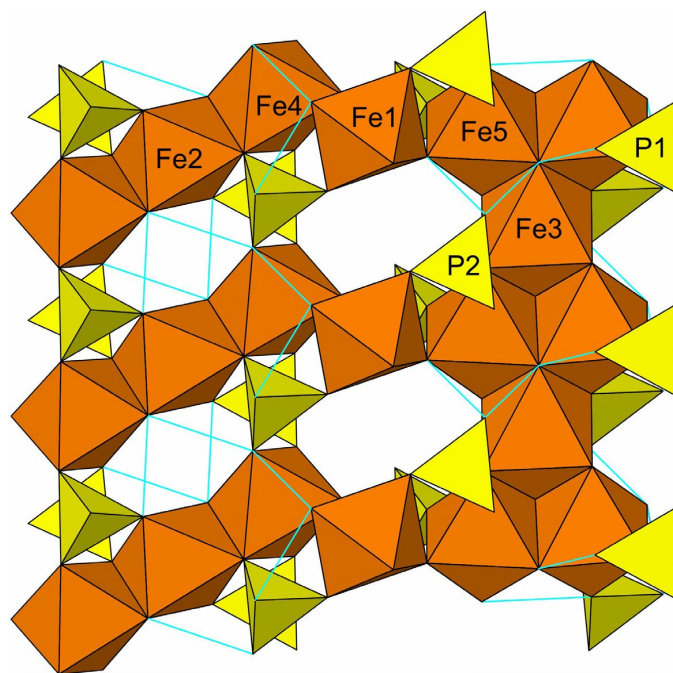
Figure 5. Octahedral–tetrahedral slice in the désorite structure viewed perpendicularly to {02$\bar{1}$} with [110] vertical. The Pb sites, which occupy the cavities, are not shown. Possible hydrogen bonds are shown as light blue lines.
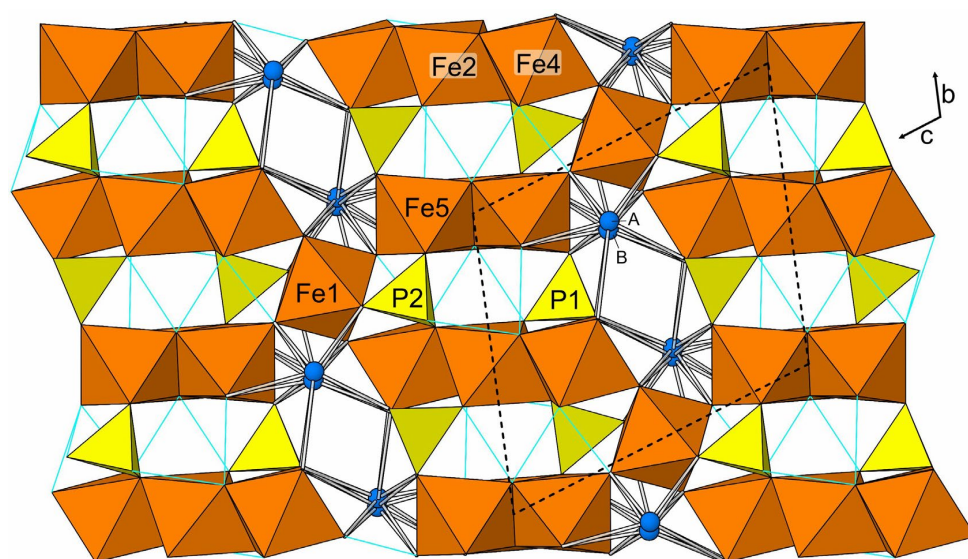
Figure 6. The structure of désorite viewed along [100]. The PbA and PbB sites are labelled A and B, respectively. Pb–O bonds are shown as sticks. Possible hydrogen bonds are shown as light blue lines. The unit-cell outline is shown with dashed lines.

7. Discussion

Désorite is isostructural with jamesite, $Pb_2ZnFe^{3+}_2(Fe^{3+},Zn)_4(AsO_4)_4(OH)_8(OH,O)_2$ [11], and lulzacite, $Sr_2Fe^{2+}_3Al_4(PO_4)_4(OH)_{10}$ [12]. Jamesite could be regarded as the arsenate analogue of désorite, except that Zn replaces Fe^{3+} as the dominant cation in the Fe2 site. (Note that our labelling of the sites in the désorite structure differs from that employed for the structure of jamesite; the désorite/jamesite octahedral-cation site correspondence is Fe1/M(3), Fe2/M(2), Fe3/M(1), Fe4/M(4), Fe5/M(5).) As in the désorite structure, the Pb site in the jamesite structure is split into two sites; interestingly, with proportions very similar to those in désorite, Pb(1a): 0.72(2); Pb(1b): 0.28(2). The separation between the split sites is also similar, 0.59(2) Å in jamesite vs 0.62(3) Å in désorite. In both structures, the Pb site splitting results in off-center Pb-O coordinations, clearly attributable to the stereoactive $6s^2$ lone-pair electrons of Pb^{2+}. By contrast, the Sr site in the luzacite structure is not split and exhibits a well-centered coordination.

Author Contributions: Conceptualization, A.R.K.; methodology, A.R.K. and C.M.; investigation, A.R.K., G.M. and C.M.; original manuscript—draft preparation, A.R.K.; manuscript—review and editing, A.R.K., G.M. and C.M.; figures, A.R.K. All authors have read and agreed to the published version of the manuscript.

Data Availability Statement: The crystallographic information file (CIF) for this paper (deposition number 2330757) are provided free of charge by the joint Cambridge Crystallographic Data Centre and Fachinformationszentrum Karlsruhe Access Structures service www.ccdc.cam.ac.uk/structures (accessed on 2 February 2024).

Conflicts of Interest: The authors declare no conflict of interest.

References

1. Pekov, I.V.; Zubkova, N.V.; Britvin, S.N.; Agakhanov, A.A.; Polekhovsky, Y.S.; Pushcharovsky, D.Y.; Möhn, G.; Desor, J.; Blass, G.A. New Mineral Hanauerite, AgHgSI, and Common Crystal Chemical Features of Natural Mercury Sulphohalides. *Crystals* **2023**, *13*, 1218. [CrossRef]
2. Seeliger, A.; Buchert, D.E.; Noll, T. Der Emser Gangzug. *Aufschluss* **2009**, *60*, 66–160.
3. Gunter, M.E.; Bandli, B.R.; Bloss, F.D.; Evans, S.H.; Su, S.C.; Weaver, R. Results from a McCrone spindle stage short course, a new version of EXCALIBR, and how to build a spindle stage. *Microscope* **2004**, *52*, 23–39.
4. Mandarino, J.A. The Gladstone–Dale compatibility of minerals and its use in selecting mineral species for further study. *Can. Miner.* **2007**, *45*, 1307–1324. [CrossRef]
5. Higashi, T. *ABSCOR*; Rigaku Corporation: Tokyo, Japan, 2001.
6. Sheldrick, G.M. SHELXT—Integrated space-group and crystal-structure determination. *Acta Crystallogr.* **2015**, *A71*, 3–8. [CrossRef] [PubMed]
7. Sheldrick, G.M. Crystal Structure refinement with SHELX. *Acta Crystallogr.* **2015**, *C71*, 3–8. [CrossRef]
8. Wright, S.E.; Foley, J.A.; Hughes, J.M. Optimization of site occupancies in minerals using quadratic programming. *Am. Mineral.* **2001**, *85*, 524–531. [CrossRef]
9. Gagné, O.C.; Hawthorne, F.C. Comprehensive derivation of bond-valence parameters for ion pairs involving oxygen. *Acta Crystallogr.* **2015**, *B71*, 562–578. [CrossRef] [PubMed]
10. Ferraris, G.; Ivaldi, G. Bond valence vs. bond length in O...O hydrogen bonds. *Acta Crystallogr.* **1988**, *B44*, 341–344. [CrossRef]
11. Cooper, M.A.; Hawthorne, F.C. Local Pb^{2+}-□ disorder in the crystal structure of jamesite, $Pb_2ZnFe^{3+}_2(Fe^{3+}_{2.8}Zn_{1.2})(AsO_4)_4(OH)_8[(OH)_{1.2}O_{0.8}]$. *Can. Mineral.* **1999**, *37*, 53–60.
12. Leone, P.; Palvadeau, P.; Moëlo, Y. Structure cristalline d'un nouvel hydroxyphosphate naturel de strontium, fer et aluminium (lulzacite), $Sr_2Fe(Fe_{0.63}Mg_{0.37})_2Al_4(PO_4)_4(OH)_{10}$. *Comptes Rendus Acad. Sci. Ser. IIC* **2000**, *3*, 301–308.